Second-order nonlinear optical properties of copper-based hybrid organic-inorganic perovskites induced by chiral amines

Bin Li,[a#] Ying Yu,[a#] Mingyang Xin,[b] Jialiang Xu,[b] Tianzhe Zhao,[a] Huimin Kang,[a] Guoxiang Xing,[a] Peisheng Zhao,[a] Tianyong Zhang*[a] and Shuang Jiang*[a]

XRD measurements: The powder X-ray diffraction data were collected by Bruker D8 Advance with Cu Kα radiation (λ = 1.5406 Å), and the thin film X-ray diffraction data were characterized by Rigaku SmartLab with Cu Kα radiation (λ = 1.5406 Å).

Single Crystal X-ray diffraction: Single crystal X-ray diffraction data were collected by Rigaku diffractometer using Kappa goniometer system equipped with an Hypix6000HE detector with a Mo Kα source (λ = 0.71073 Å) at 200 K. The bulk crystals are cut into small ones and the right micron-sized crystals (about 0.15 × 0.15 × 0.15 mm) are selected under the microscope.

Magnetic characterization: The SQUID-VSM magnetic measurement system has been used to characterize the magnetic properties of (R-/S-NEA)$_2$CuCl$_4$ and (R-/S-CYHEA)$_6$Cu$_3$Cl$_{12}$ bulk single crystals. Temperature-dependent magnetic flux curves were obtained with magnetic field of 10000 Oe. The magnetic-field dependent magnetic flux curves were tested with the temperature range of 2-30 K.

Linear optical measurements: Infrared spectrometry spectra were recorded by a Fourier transformation infrared spectrometer (FTIR, Thermo Fisher SCIENTIFIC, Nicolet). The UV-Vis spectra of single crystals were measured by Hitachi U-3010 UV–visible-spectrometer. The samples were ground into powder with $BaSO_4$ as the background. CD and the UV-Vis absorbance data were collected by Jasco J-810 spectrometer. The g-factor is calculated by the equation as followed:

$$g_{CD} = \frac{CD(mdeg)}{32982A}$$

Where CD is the absorption difference between the left and right circularly polarized light, and A refers to the absorption of the total incident light.

NLO Measurements: The NLO properties of chiral perovskite thin films were studied with a home-built set-up with a femtosecond laser pump (Mai Tai HP, 100 fs, 80 MHz, 800-1040 nm). The measurements were conducted under a reflection geometry at a 45 ° angle of both incidence and detection.

The calculation of NLO coefficient I: The effective NLO coefficient of $(R\text{-}NEA)_2CuCl_4$ and $(R\text{-}CYHEA)_6Cu_3Cl_{12}$ thin films are calculated by using Y-cut quartz as reference. The formula is as follows[1](p refers to perovskite thin film and q refers to Y-cut quartz):

$$\frac{d_{eff}^{p}}{d_{eff}^{q}} = \sqrt{\frac{I_{2\omega}^{p} I_{\omega}^{q} L^{q} n_{\omega}^{p}}{I_{2\omega}^{q} I_{\omega}^{p} L^{p} n_{\omega}^{q}}} \sqrt{\frac{n_{2\omega}^{p}}{n_{2\omega}^{q}}}$$

Here, $I_{2\omega}$ is the SHG response, I_{ω} is the incident light intensity, L is the effective crystal thickness, and n_{ω} and $n_{2\omega}$ are the refractive indices at the frequency ω and 2ω. The refractive indices for quartz are 1.552 and 1.535 at 460 nm and 920 nm[2] and that of $(R\text{-}NEA)_2CuCl_4$ thin film were measured to be 1.740 and 1.591 at 460 nm and 920 nm, and $(R\text{-}CYHEA)_6Cu_3Cl_{12}$ thin film were 1.708 and 1.648, respectively. Herein, we think of the thickness of Y-cut quartz is equal to perovskite films. The SHG signals of these samples were collected by using the same measurement conditions under 920 nm, 50 mW excitation. Therefore, $I_{\omega}^{p} = I_{\omega}^{q}$. The detected SHG intensitis of Y-cut quartz, $(R\text{-}NEA)_2CuCl_4$ and $(R\text{-}CYHEA)_6Cu_3Cl_{12}$ thin film are 8825, 39259 and 2465.7 cps, respectively. d_{eff}^{q} is 0.6 pm V^{-1}. Thus, the NLO coefficient of $(R\text{-}NEA)_2CuCl_4$ thin film is determined to be 2.31 pm V^{-1}, and the NLO coefficient of $(R\text{-}CYHEA)_6Cu_3Cl_{12}$ thin film is determined to be 0.60 pm V^{-1}.

The calculation of NLO coefficient II: The effective NLO coefficient of $(R\text{-}NEA)_2CuCl_4$ and $(R\text{-}CYHEA)_6Cu_3Cl_{12}$ thin films are calculated by using Y-cut quartz as a reference. According to Xu's work[3], the electric field of reflected SHG intensity of perovskite films can be calculated by the equation[4]:

$$E_{rp} = \frac{n_{\omega}cos\theta - n_{2\omega}cos\theta_{t}}{cos\theta + n_{2\omega}cos\theta_{r}} \times \frac{P_{NLp}^{(2)}}{\varepsilon(n_{\omega}^{2} - n_{2\omega}^{2})} + \frac{n_{2\omega}sin\theta_{t}}{cos\theta + n_{2\omega}cos\theta_{r}} \times \frac{P_{NLt}^{(2)}}{\varepsilon n_{2\omega}^{2}}$$

Where $P_{NLp}^{(2)}$ is the second-order nonlinear polarization parallel to the p-polarization of the transmitted fundamental wavelength and $P_{NLt}^{(2)}$ is the second-order nonlinear polarization parallel to the direction of the transmitted fundamental wavelength propagation, n_ω and $n_{2\omega}$ are the refractive indices at the frequency ω and 2ω. θ_r is the reflection angle, and θ_i is the incident angle. θ_t is the refraction angle of fundamental wavelength and θ is the angle of the SHG wavelength. These angles can be calculated by the following formula: $n_\omega sin\theta_t = n_{2\omega} sin\theta = sin\theta_r = sin\theta_i$

For quartz, β refers to the NLO susceptibility, and β=0.6 pm V^{-1}.

$$P_{NLp,q}^{(2)} = -\varepsilon((E_X^2 - E_y^2)cos\theta_t + 2E_xE_y sin\theta_t)\beta$$

$$P_{NLt,q}^{(2)} = \varepsilon((E_X^2 - E_y^2)sin\theta_t - 2E_xE_y cos\theta_t)\beta$$

where E_x and E_y are the electric fields of the fundamental pump in quartz, which can be described by Fresnel formula:

$$E_x = \frac{2cos\theta_i cos\theta_t}{cos\theta_t + n_\omega cos\theta_i}E_i$$

$$E_y = -\frac{2cos\theta_i sin\theta_t}{cos\theta_t + n_\omega cos\theta_i}E_i$$

The refractive indices for quartz are 1.552 and 1.535 at 460 nm and 920 nm, $\theta_i=\theta_r=45$ °, $\theta_t=27.41$ °, $\theta=27.10$ °.

$$E_{rp,q} = 0.4484\beta E_i^2$$

For perovskite, we assumed that the $P_{NLt}^{(2)}$ is negligible and $P_{NLp}^{(2)} = \varepsilon d_{eff} E_p^2$

$$E_p = \frac{2cos\theta_i}{cos\theta_t + n_\omega cos\theta_i}E_i$$

The refractive indices of $(R\text{-}NEA)_2CuCl_4$ thin film were measured to be 1.740 and 1.591 at 460 nm and 920 nm, respectively. $\theta_i=\theta_r=45$ °, $\theta_t=26.39$ °, $\theta=23.98$ °.

So $E_{rp,R-NEA} = 0.04833 d_{eff} E_i^2$. The detected SHG intensitis of Y-cut quartz and (R-NEA)$_2$CuCl$_4$ thin film are 8825, 39259 cps, respectively. Therefore, the d_{eff} of (R-NEA)$_2$CuCl$_4$ thin film is determined to be 11.74 pm V^{-1}.

The refractive indices of (R-CYHEA)$_6$Cu$_3$Cl$_{12}$ thin film were measured to be 1.760 and 1.852 at 460 nm and 920 nm, respectively. θ_i=θ_r=45 °, θ_t=25.41 °, θ=24.46 °. So $E_{rp,R-CYHEA} = 0.04677 d_{eff} E_i^2$.

The detected SHG intensitis of (R-CYHEA)$_6$Cu$_3$Cl$_{12}$ thin film are 2465.7 cps. So the d_{eff} of (R-CYHEA)$_6$Cu$_3$Cl$_{12}$ thin film is determined to be 3.04 pm V^{-1}.

Table S1 Crystal data and structure refinement for (R-/S-NEA)$_2$CuCl$_4$.

Identification code	(R-NEA)$_2$CuCl$_4$	(S-NEA)$_2$CuCl$_4$
Empirical formula	$C_{24}H_{28}Cl_4CuN_2$	$C_{24}H_{28}Cl_4CuN_2$
Formula weight	549.859	549.859
Temperature/K	199.99(10)	199.98(10)
Crystal system	monoclinic	monoclinic
Space group	P2$_1$	P2$_1$
a/Å	12.6402(4)	12.6550(3)
b/Å	7.1773(2)	7.1832(2)
c/Å	14.0019(4)	13.9997(3)
α/°	90	90
β/°	94.296(3)	94.341(2)
γ/°	90	90
Volume/Å^3	1266.72(7)	1268.97(5)
Z	2	2
ρ_{calc}g/cm^3	1.442	1.439
μ/mm^{-1}	1.299	1.296
F(000)	568.0	568.0
Crystal size/mm^3	0.15 × 0.15 × 0.15	0.150 × 0.150 × 0.150
Radiation	Mo Kα (λ = 0.71073)	Mo Kα (λ = 0.71073)
2Θ range for data collection/°	4.18 to 61.12	4.18 to 61.2
Index ranges	-17 ≤ h ≤ 17, -9 ≤ k ≤ 10, -19 ≤ l ≤ 17	-17 ≤ h ≤ 15, -10 ≤ k ≤ 10, -18 ≤ l ≤ 19

Reflections collected	18221	16628
Independent reflections	6385 [R_{int} = 0.0267, R_{sigma} = 0.0296]	6250 [R_{int} = 0.0263, R_{sigma} = 0.0286]
Data/restraints/parameters	6385/1/146	6250/1/130
Goodness-of-fit on F^2	1.012	2.693
Final R indexes [I>=2σ (I)]	R_1 = 0.0813, wR_2 = 0.1951	R_1 = 0.1777, wR_2 = 0.5066
Final R indexes [all data]	R_1 = 0.0838, wR_2 = 0.1973	R_1 = 0.1804, wR_2 = 0.5143
Largest diff. peak/hole / e $Å^{-3}$	4.06/-1.99	13.95/-1.93
Flack parameter	0.028(4)	0.112(4)

Table S2 Crystal data and structure refinement for (R-/S-CYHEA)$_6$Cu$_3$Cl$_{12}$.

Identification code	(R-CYHEA)$_6$Cu$_3$Cl$_{12}$	(S-CYHEA)$_6$Cu$_3$Cl$_{12}$
Empirical formula	$C_{48}H_{108}Cl_{12}Cu_3N_6$	$C_{48}H_{108}Cl_{12}Cu_3N_6$
Formula weight	1385.42	1385.42
Temperature/K	200	200.00(10)
Crystal system	monoclinic	monoclinic
Space group	I2	I2
a/Å	20.4991(7)	20.4795(5)
b/Å	18.1779(6)	18.1694(4)
c/Å	19.6327(7)	19.6068(6)
α/°	90	90
β/°	107.114(4)	107.039(3)
γ/°	90	90
Volume/Å^3	6978.3(8)	6975.5(3)
Z	4	4
ρ_{calc}g/cm^3	1.319	1.319
μ/mm^{-1}	5.544	1.400
F(000)	2916.0	2916.0
Crystal size/mm^3	0.15 × 0.15 × 0.15	0.15 × 0.15 × 0.15
Radiation	MoKα (λ = 0.71073)	Mo Kα (λ = 0.71073)
2Θ range for data collection/°	5.546 to 134.158	4.16 to 61.51
Index ranges	-24 ≤ h ≤ 24, -21 ≤ k ≤ 21, -22 ≤ l ≤ 23	-27 ≤ h ≤ 28, -25 ≤ k ≤ 25, -24 ≤ l ≤ 26
Reflections collected	86146	65436
Independent reflections	12326 [R_{int} = 0.0915, R_{sigma} =	17343 [R_{int} = 0.0402, R_{sigma} = 0.0409]

	0.0391]	
Data/restraints/parameters	12326/575/637	17343/795/666
Goodness-of-fit on F^2	1.097	1.089
Final R indexes [I>=2σ (I)]	R_1 = 0.0640, wR_2 = 0.1851	R_1 = 0.0398, wR_2 = 0.1078
Final R indexes [all data]	R_1 = 0.0743, wR_2 = 0.1940	R_1 = 0.0550, wR_2 = 0.1144
Largest diff. peak/hole / e Å^{-3}	0.57/-0.77	0.53/-0.45
Flack parameter	0.07(3)	0.013(6)

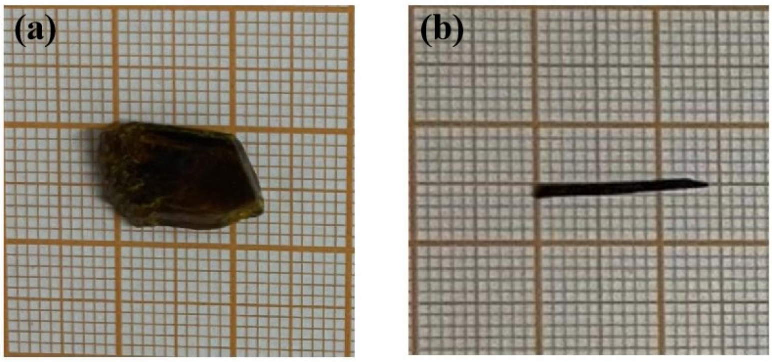

Figure S1 The digital photograph of (a) (R-NEA)$_2$CuCl$_4$ single crystal. (b) (R-CYHEA)$_6$Cu$_3$Cl$_{12}$ single crystal.

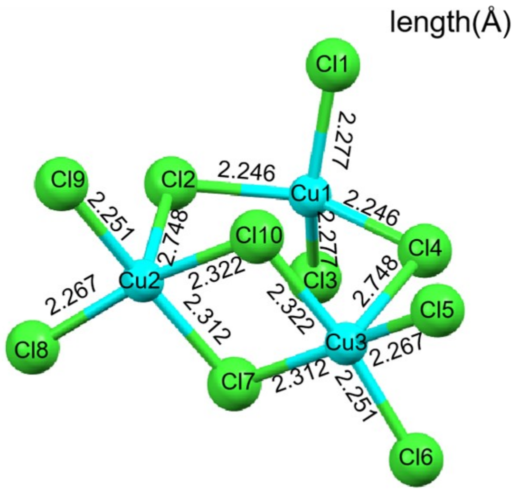

Figure S2 The distorted [Cu$_3$Cl$_{10}$]$^{4-}$ structure of (R-CYHEA)$_6$Cu$_3$Cl$_{12}$.

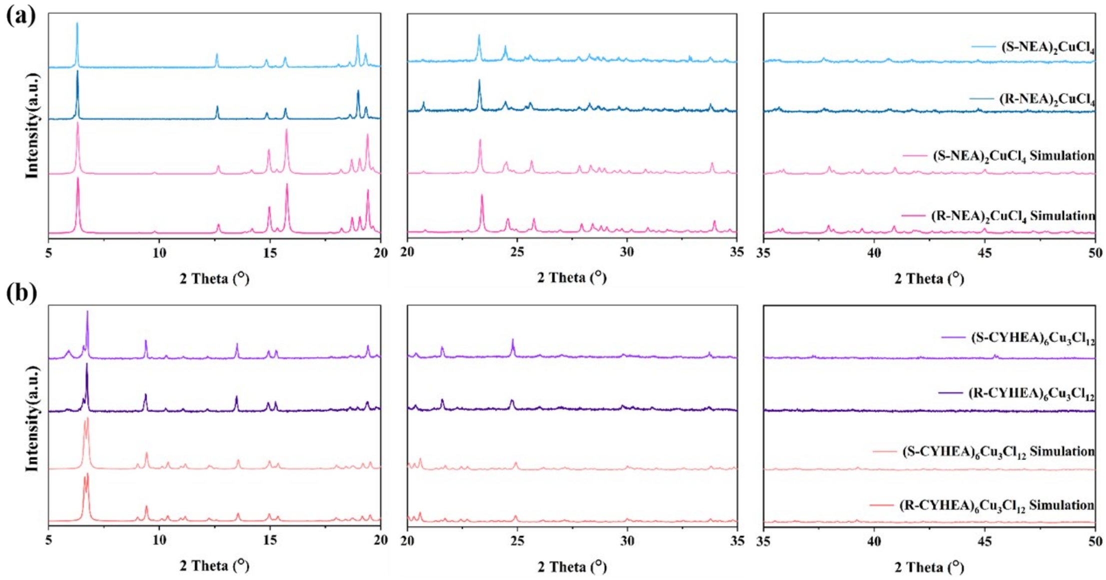

Figure S3 The zoomed-in regions of PXRD patterns of (a) (R-NEA)$_2$CuCl$_4$ and (b) (R-CYHEA)$_6$Cu$_3$Cl$_{12}$.

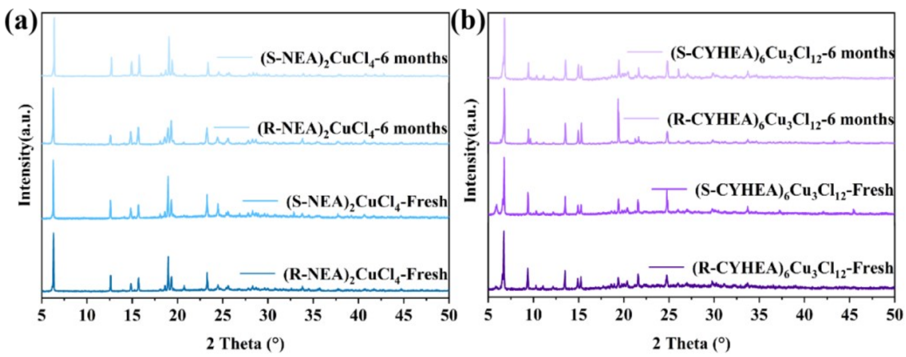

Figure S4 The PXRD patterns of (a) (R-/S-NEA)$_2$CuCl$_4$ and (b) (R-/S-CYHEA)$_6$Cu$_3$Cl$_{12}$ single crystals before and after stored in the air for 6 months.

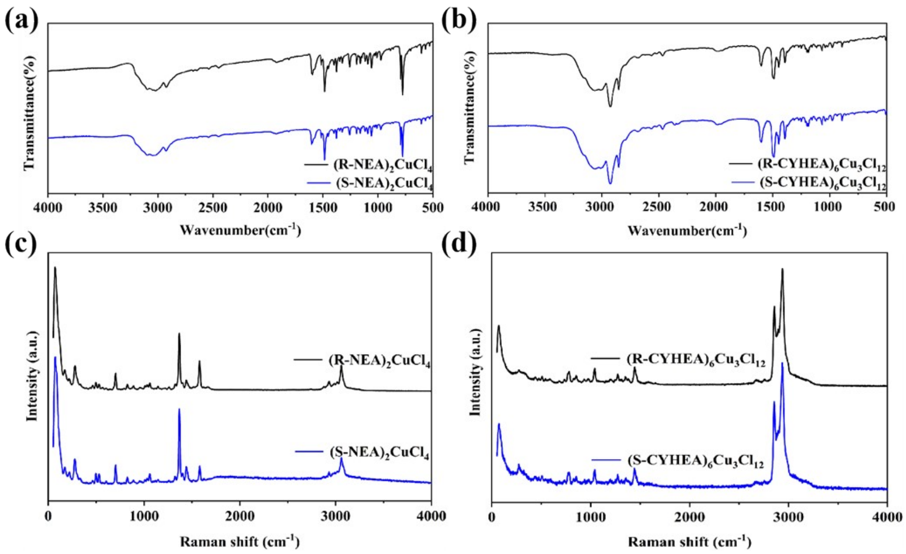

Figure S5 The FTIR spectra of (a) (R-/S-NEA)$_2$CuCl$_4$ and (b) (R-/S-CYHEA)$_6$Cu$_3$Cl$_{12}$ single crystals. The Raman spectra of (c) (R-/S-NEA)$_2$CuCl$_4$ and (d) (R-/S-CYHEA)$_6$Cu$_3$Cl$_{12}$ single crystals.

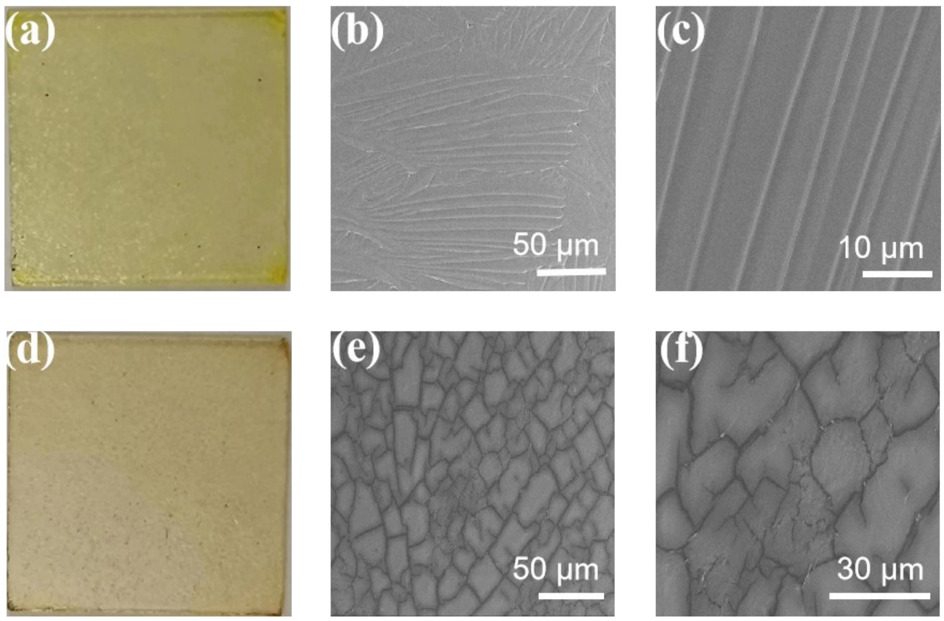

Figure S6 The digital photo of (a) (R-NEA)$_2$CuCl$_4$ and (d) (R-CYHEA)$_6$Cu$_3$Cl$_{12}$ thin films. The SEM image of (b, c) (R-NEA)$_2$CuCl$_4$ and (e, f) (R-CYHEA)$_6$Cu$_3$Cl$_{12}$ thin films.

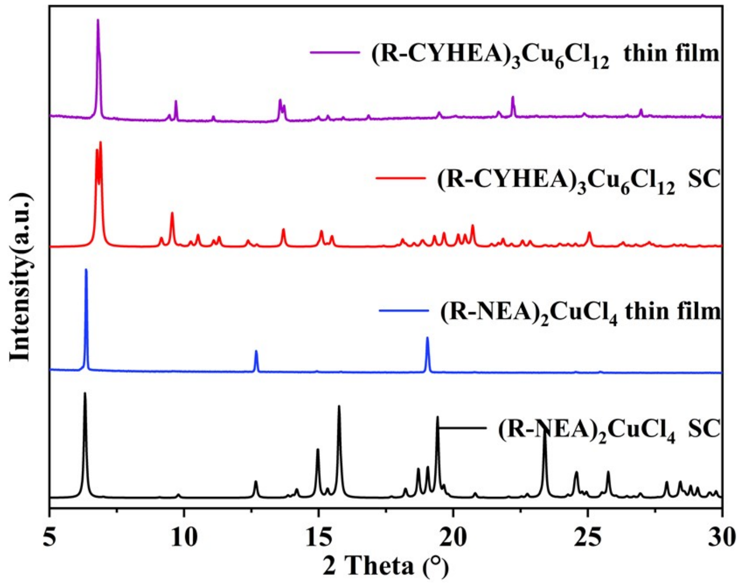

Figure S7 The XRD patterns of (R-NEA)$_2$CuCl$_4$ and (R-CYHEA)$_6$Cu$_3$Cl$_{12}$ thin films in comparison to their single crystals.

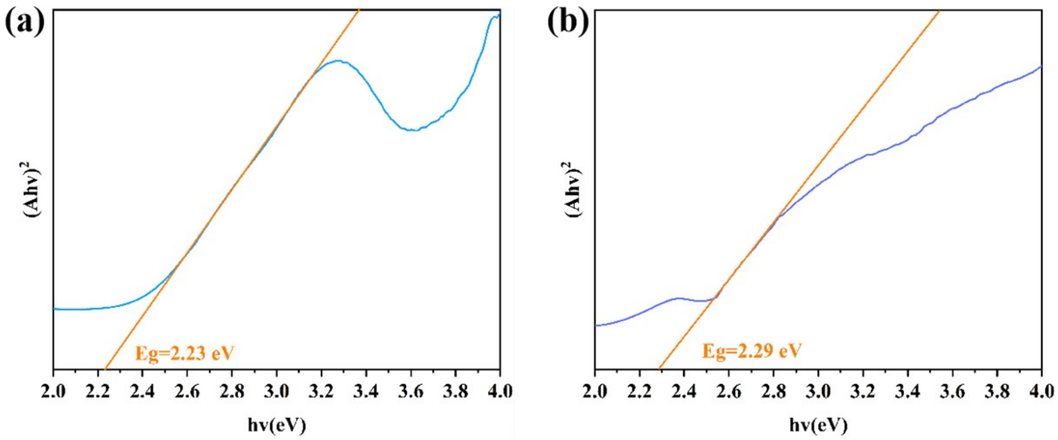

Figure S8 The Tauc Plots of (a) (R-NEA)$_2$CuCl$_4$ and (R-CYHEA)$_6$Cu$_3$Cl$_{12}$.

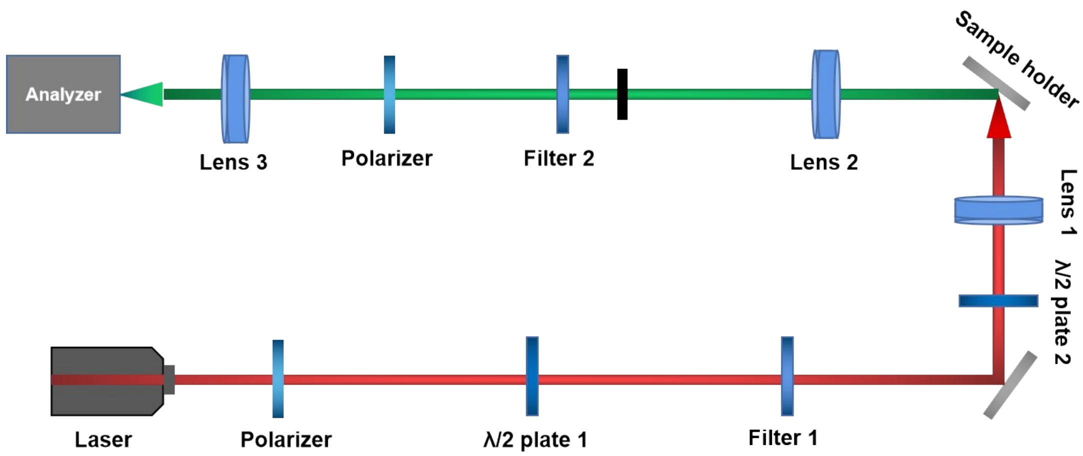

Figure S9 The diagram of home-built optical setup with a femtosecond pulsed laser.

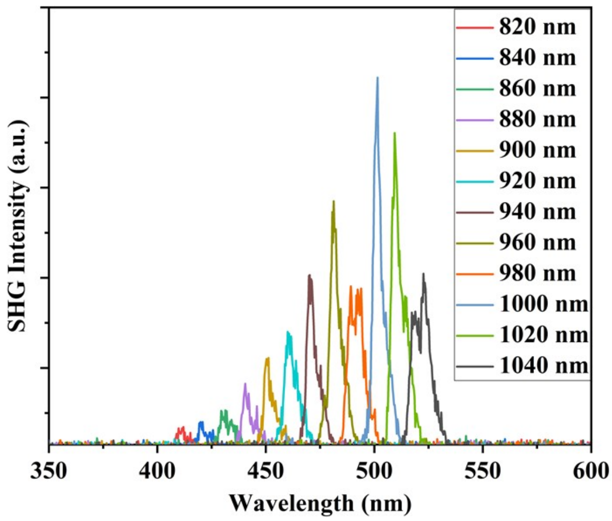

Figure S10 The wavelength-dependent SHG response of Y-cut quartz.

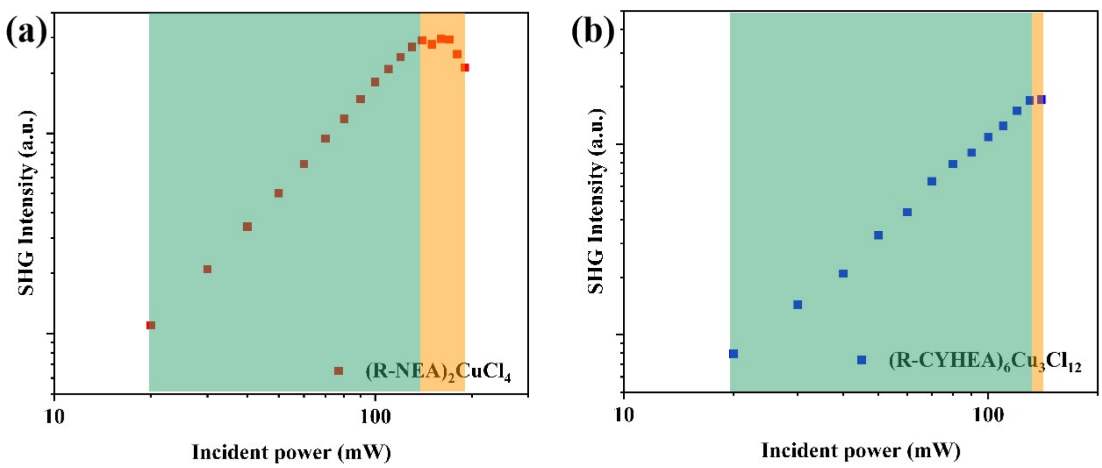

Figure S11 The pumping power-dependent SHG response of (a) $(R\text{-}NEA)_2CuCl_4$ and (b) $(R\text{-}CYHEA)_6Cu_3Cl_{12}$ thin film. The green region indicates the quadratic dynamic range and the yellow region indicates the damage region.

1. Y. Duan, C. Ju, G. Yang, E. Fron, E. Coutino-Gonzalez, S. Semin, C. Fan, R. S. Balok, J. Cremers and P. Tinnemans, *Adv. Funct. Mater.*, 2016, **26**, 8968-8977.
2. G. Ghosh, *Opt. Commun.*, 1999, **163**, 95-102.
3. Y. Zheng, J. Xu and X. H. Bu, *Adv. Opt. Mater.*, 2022, **10**, 2101545.
4. W. T. Welford, *Phys. Bull.*, 1985, **36**, 178-178.